Electronic Supplementary Material (ESI) for Journal of Materials Chemistry A.

Supporting Information

Exploring Low-Cost High Energy NASICON- Cathodes for Sodium-Ion Batteries via a Combined Machine-Learning, *Ab Initio*, and Experimental Approaches†

Vaiyapuri Soundharrajan,[a] *Muhammad Hilmy Alfaruqi,*[a,b] *Ghalib Alfaza,*[a] *Jun Lee,*[a] *Seulgi Lee,*[a] *Sohyun Park,*[a] *Subramanian Nithiananth,*[c] *Duong Tung Pham,*[d] *Jang-Yeon Hwang*[e,]* *and Jaekook Kim*[a,f]*

[a]Department of Materials Science and Engineering, Chonnam National University, 300 Yongbong-dong, Bukgu, Gwangju 500-757, South Korea
[b]Department of Metallurgical Engineering, Sumbawa University of Technology, Olat Maras, Sumbawa, West Nusa Tenggara, 84371, Indonesia
[c]Graduate School of Science and Technology, Shizuoka University, 3-5-1 Johoku, Naka-ku, Hamamatsu, Shizuoka, 432–8011, Japan
[d]School of Engineering Physics, Hanoi University of Science and Technology, No 1 Dai Co Viet Street, 100000, Hanoi, Viet Nam
[e]Department of Energy Engineering, Hanyang University, Seoul 04763, South Korea
[f]Research Center for Artificial Intelligence Assisted Ionics Based Materials Development Platform, Chonnam National University, Gwangju, 61186, South Korea

*E-mail: jaekook@chonnam.ac.kr

Experimental section

NMVTP/C was synthesized through a rapid, modified pyro-synthesis approach. In 100 mL of tetraethylene glycol, 3.5 mmol of sodium nitrate (Sigma-Aldrich, 99 %), 1 mmol of manganese nitrate (Sigma-Aldrich, 97 %), and 0.5 mmol of titanium isopropoxide (Sigma-Aldrich, 99.99 %) were dissolved to obtain solution A. In a solution of 5 mL of deionized water and 1 mmol of the reducing agent oxalic acid (DAEJUNG, 99.5 %), 0.5 mmol of ammonium vanadate (JUNSEI, 99 %) was dissolved to obtain solution B. Oxalic acid promotes the reduction of V^{5+} to V^{3+}. Solution B was added to solution A, and 3 mmol of phosphoric acid (DAEJUNG, 85 %) was stirred into the resulting solution to obtain a polyol stock solution. The stock solution was transferred into an aluminum boat on a hot plate at 450 °C and was ignited using an electric torch to trigger the rapid self-extinguishing combustion process. Finally, the combustion deposits were collected and annealed at 600 °C in the Ar atmosphere for 10 h to obtain the carbon-coated NMVTP/C micro-flakes. Likewise, NMVFP/C and NMVAP/C were also synthesized via a similar approach, where iron nitrate nonahydrate (Sigma-Aldrich, 98 %) and aluminum nitrate nonahydrate (Sigma-Aldrich, 98 %) were used as a source for Fe and Al.

Structural and physical characterization

The crystal structure was identified using a 3D high-resolution X-ray diffractometer (Empyrean, PANalytical, The Netherlands). Powder X-ray diffraction (PXRD) patterns were obtained using a Shimadzu X-ray diffractometer (Cu Kα radiation, $\lambda = 1.5406$ Å). The morphology of the synthesized materials was observed through Field Emission Scanning Electron Microscopy (FESEM) using an S-4700 Hitachi with an Energy Dispersive X-ray Spectroscopic detector (EDS). Furthermore, High Resolution Transmission Electron Microscopy (HRTEM, 20 kV, Philips Tecnai F20, KBSI Chonnam National University) with Selected Area Electron Diffraction was employed to analyze the lattice fringes. X-ray photoelectron spectroscopy (XPS, Thermo VG Scientific Multilab 2000) with an Al Kα X-ray source was utilized to determine the elemental surface oxidation states of the NMVTP/C sample. The calibration was performed with a C 1s binding energy at 284.6 eV. The carbon content in the NMVTP/C sample was calculated from the thermogravimetric analysis (TGA) using an SDT Q600 thermobalance in the air with a temperature gradient of 5 °C min^{-1}. A JASCO Laser Raman Spectrometer NRS-5100 series was used to obtain the Raman spectra to identify the nature of the carbon in the samples.

Electrochemical characterization

For the assembly of half-cells, the positive electrode was fabricated by mixing 70 % of the active material, 20 % of Ketjen black, and 10 % of polyacrylic acid, creating a slurry with 5 wt% of the resulting mixture with the N-methyl-2-pyrrolidone solvent, and casting the slurry onto aluminum foil. Following this, the electrodes were dried in a vacuum at 80 °C, and the dried foil was hot-pressed between stainless steel rollers at 120 °C and punched into round disks with a diameter of 14 mm. CR-2032 coin-type cells were fabricated using Na metal as the reference/counter electrode and glass fiber as the separator in an Ar-filled glove box. The electrolyte used was 1 M $NaPF_6$ in ethylene carbonate/diethylene carbonate with a 5 % fluoroethylene carbonate additive. The cells were aged overnight before testing to ensure the complete absorption of the electrolyte into the electrodes. Full-cells were constructed using CR-2032 coin-type cells and employed $Na_{3.5}MnV_{0.5}Ti_{0.5}(PO_4)_3$ as the cathode and hard carbon as the anode. The hard carbon anode is chemically sodiated before assembly by paring with the metallic sodium anode (electrolyte is packed in between) for 1 h; recovered and used for full-cell construction. And the full-cell system balance is accomplished by regulating the capacity ratio of cathode/anode to about 1.2. The same electrolyte and separator that were employed for half-cell construction were used for the Full-cell assembly. A BTS 2004H model (NAGANO KEIKI Co., LTD, Ohta-ku Tokyo, Japan) battery testing system was used to perform the galvanostatic charge/discharge measurements at various current rates between 4.15 and 1.5 V. Cyclic voltammetry (CV) and GITT studies were performed using apparatus from BioLogic Science Instruments.

In situ XRD studies

In situ XRD examination of the NMVTP/C sample during galvanostatic cycling was performed using a self-designed *in situ* cell. I*n situ* XRD setup involves a special split test cell was employed with a beryllium window for X-ray penetration. For the *in situ* cell, the electrode was made-up by mixing 70 % of the active material, 20 % of Ketjen black, and 10 % of the teflonated acetylene black binder and pressing the mixture onto an aluminum mesh, was applied onto a beryllium (Be) serving as both current collector and the X-ray penetration window. Metallic sodium disc worked as a counter electrode, Whatman glass fiber as a separator, and 1 M $NaPF_6$ in ethylene carbonate/diethylene carbonate with 5 % fluoroethylene carbonate additive as an electrolyte. The *in situ* cell was galvanostatically charged and discharged at a current density of 0.07 C between 4.15-1.5 V. The *in situ* XRD outputs were recorded using laboratory diffractometers by means of Mo K_α radiation in reflection geometry and each array took 2 min to record the patterns. The recorded Mo K_α radiation patterns were converted into Cu K_α radiation patterns using the inbuild X'Pert Highscore Plus Program.

Machine learning

The machine-learning method was executed in a Python program using the Jupyter Notebook interface. We retrieved the Materials Project database of formation energy per atom using matminer.data_retrieval.retrieve_MP.[1] The criteria used to retrieve the data was "nelements" with the value of 1, 2, 3, and 4. XG Boost (XGB), Random Forest (RF), Bayesian Ridge (BR), and Support Vector Machine (SVM) Regressions algorithms were used to train the model. For the train-test split, we used a test size of 0.33 and a random state of 42. Before implementing the algorithm, datasets were scaled and normalized using StandardScaler and Normalizer, respectively.

First-principles calculations

Quantum-Espresso package with projector augmented wave (PAW), pseudopotential and Perdew–Burke–Ernzerhof (PBE) exchange-correlation functional was used to perform first-principles calculations based on density functional theory (DFT).[2-4] The "vc-relax" function and Broyden–Fletcher–Goldfarb–Shanno (BFGS) were used to allow the optimization of 2 units cell of NMVTP which consists of 42 atoms with a plane-wave basis set with a kinetic energy of 680 eV and the convergence threshold was set to 1.0E-06. For further convex hull calculation, the lowest energy from 10 different NMVTP configurations with the lowest electrostatic energies generated by Supercell software developed by Okhotnikov et al.[5] was selected. The Brillouin zones were sampled using 2 x 2 x 1 *k*-point with an energy convergence of 1.3 meV and force convergence of 26 meV/Å thresholds.[3,4] Using only a generalized gradient approximation (GGA) to account for the correlation error in 3d orbitals, the calculation of structures that involve transition metals and oxygen encounters several issues. The Hubbard U correction was used for Mn, V, and Fe with values of 3.9, 3.25, and 4.0, respectively and Na diffusion analysis was evaluated using SoftBV software. While for Ti, we did not include any Hubbard correction since Ti oxides show weakly localized d-orbital electrons, and may not exhibit as strong correlations as manganese, vanadium, or iron, and titanium is metallic in its reduced state, hence, making the Hubbard correction less critical for titanium-based systems.[6] All of the U values were given according to the previous report.[6] Note that, in this study, we did not apply dispersion correction. Dispersion correction is effective to solve some long-range correction problems such as response properties such as spectroscopic constants, electronic excitation spectra, and weakly-bonded structures of large systems.[7] In this study, we did not consider the NASICON structures as a weakly-bonded system where the major interaction between atoms is strong covalent-bonded, for instance, the tetrahendron anion units $(PO_4)^{3-}$ and MO_x polyhedral (M represents a transition metal). Even though there was a new report regarding the utilization of vdW dispersion correction, the mechanism of how vdW dispersion could improve the accuracy of DFT calculation to predict the properties of NASICON as electrode materials were unclear in the report.[8] For a better prediction by density functional theory, we could utilize other functionals such as SCAN and HSE06 but the computational cost must be extremely expensive considering the complexity of the NASICON structure.[9] To minimize the discrepancies, we therefore utilized Hubbard correction which is widely implemented for electrode calculations to predict the electrochemical properties despite the slight inaccuracy of the result. Nevertheless, we argue that the error between the prediction and the experimental result is still tolerable. Na diffusion analysis was evaluated using SoftBV software.[10]

Theoretical capacity calculation

Theoretical capacity can be determined from the no of moles of electrons involved in the reaction as per the Faradays law[7]:

Theoretical capacity, $T_C = 26800$ n/M

At a low current rate, the $Na_{3.5}MnV_{0.5}Ti_{0.5}(PO_4)_3$ cathode can supply a capacity of 133.14 mAh g^{-1}, which indicates that 2.36 moles of Na^+ ions participated in the capacity output, demonstrating the multielectron involvement. Since V and Ti amount is limited, the complete 3-electron reaction is not viable, this indicates that 2.5 moles of Na^+ ions could participate accordingly, the theoretical capacity of NMVTP can be found as 142.68 mAh g^{-1} i.e., (1 C =142.68 mAh g^{-1}). In addition, the theoretical capacity of NMVAP and NMVFP can be found as 145.6 mAh g^{-1} and 141.5 mAh g^{-1}, respectively.

Specific power and specific energy calculation

Specific energy can be determined from the capacity and voltage output of the cathode[7]:

Specific energy E (Wh kg^{-1}) = Specific capacity x voltage (average working voltage)

Specific power can be determined from the applied current density and voltage output of the cathode[7]:

Specific power P (W kg^{-1}) = I x V/2*m*, Where I is the applied current (A), V is the average working voltage (V), and *m* is the active mass on the cathode side[8].

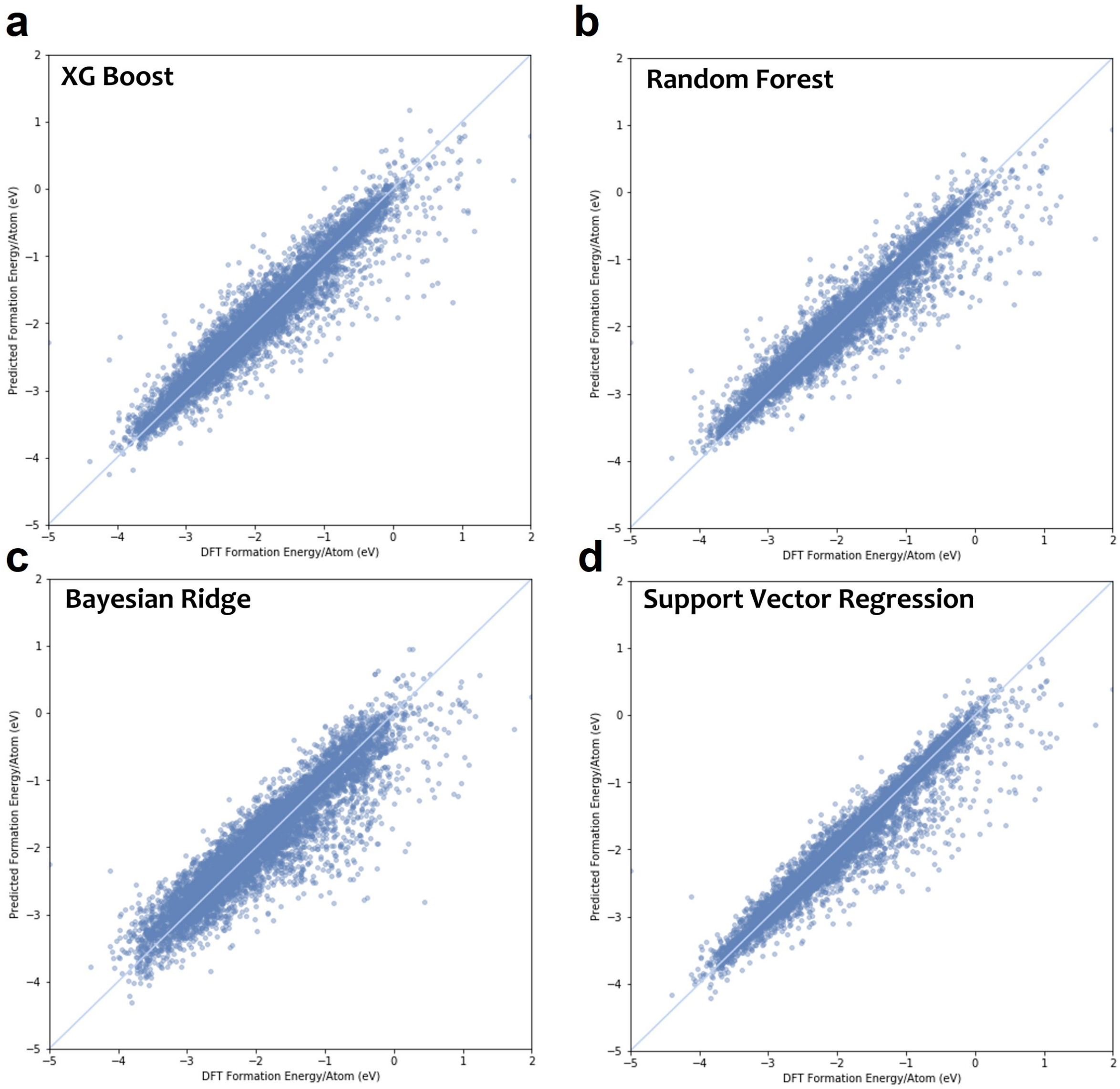

Fig. S1. Scatter plot showing DFT-calculated vs. ML-predicted formation energy per atom using (a) XG Boost, (b) Random Forest, (c) Bayesian Ridge, and (d) Support Vector Regression algorithms.

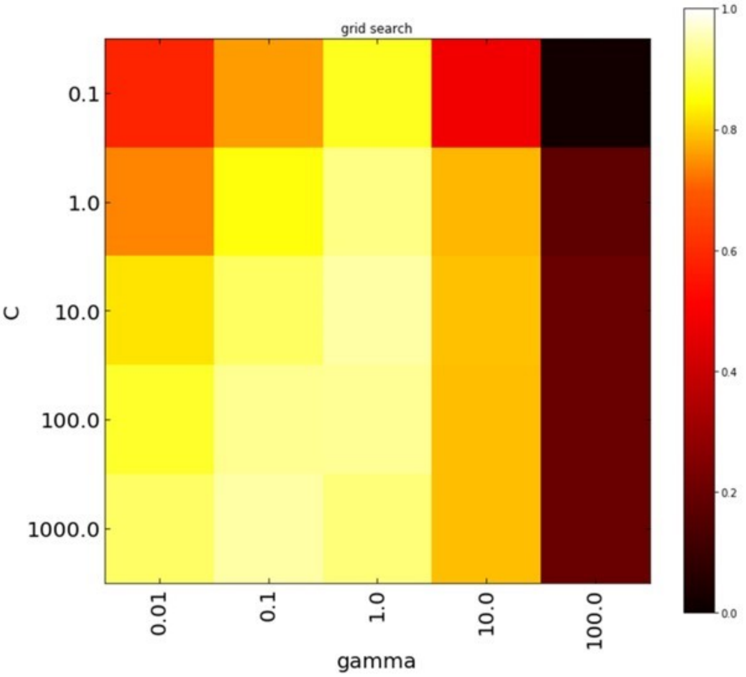

Fig. S2. Hyperparameter c and gamma tuning result heat map plot using GridSearch.

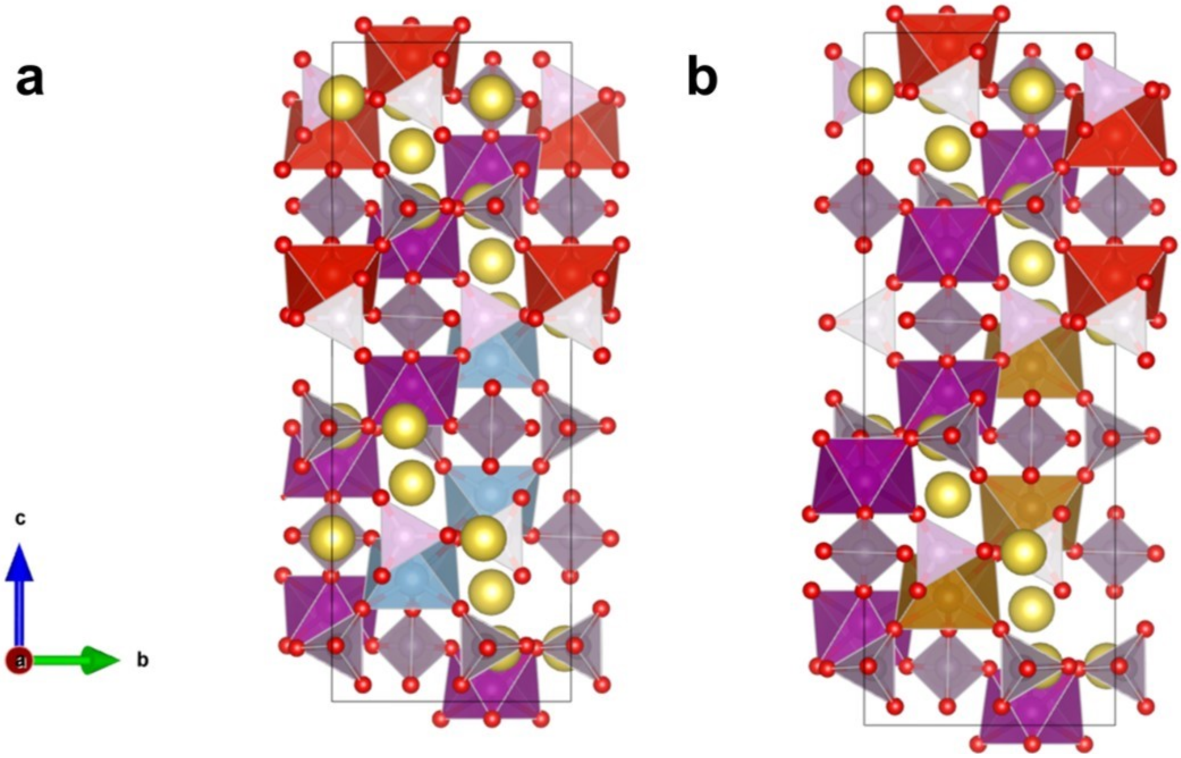

Fig. S3. DFT predicted (a) NMVAP and (b) NMVFP.

Table S1. Comparison of lattice parameters of the proposed compounds obtained from DFT calculations.

Material	a	b	c	α	β	γ
NMVAP	8.98768	8.99277	21.47619	89.9142	90.0737	119.9723
NMVFP	9.42037	9.42182	22.50501	89.9948	90.0156	120.0059
NMVTP	9.47602	9.48161	22.50751	90.0992	89.8899	120.0612

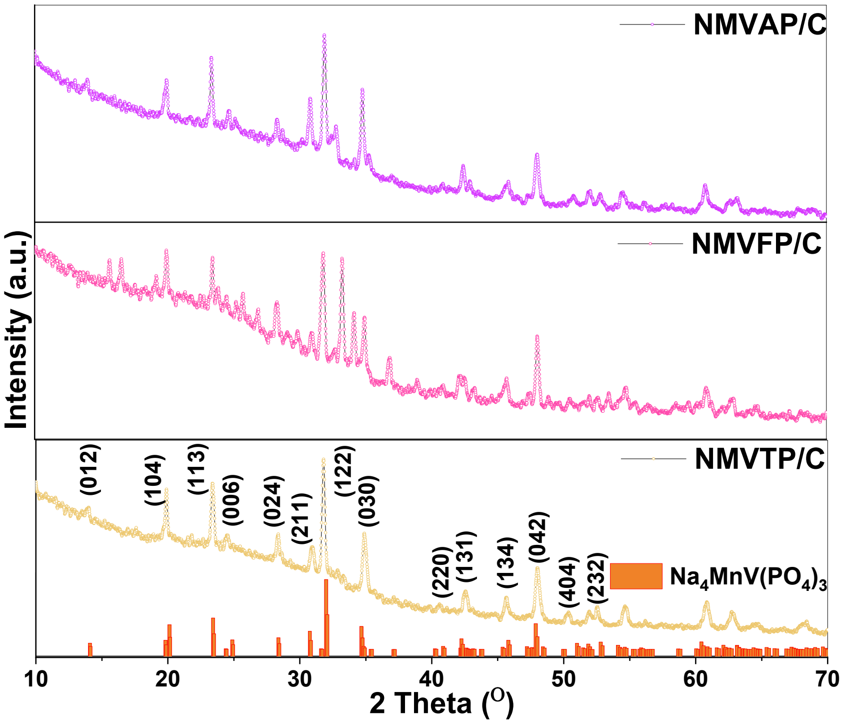

Fig. S4. Comparison of XRD patterns of the proposed compounds obtained from DFT calculations.

Table S2 Crystallographic data of the NMVTP/C cathode obtained from Rietveld refinement.

Element	Wyckoff Positions			SOF	Biso
	x	y	Z		
Na	0	0	0	0.99641	2.64602
Na	0.6425	0	0.25	0.81685	1.51747
Mn	0	0	0.14901	0.5	1
V	0	0	0.14901	0.25	1
Ti	0	0	0.14901	0.25	0.5
P	0.298	0	0.25	1	1
O	0.0136	0.209	0.1932	1	1
O	0.1863	0.1721	0.0852	1	1
R_{wp} = 10.977, R_p = 10.303, R_{exp} = 8.606, GoF = 1.62					
a = b = 8.85431 Å, c = 21.68460 Å; α = β =90˚, γ = 120˚ V=1472.285 Å					

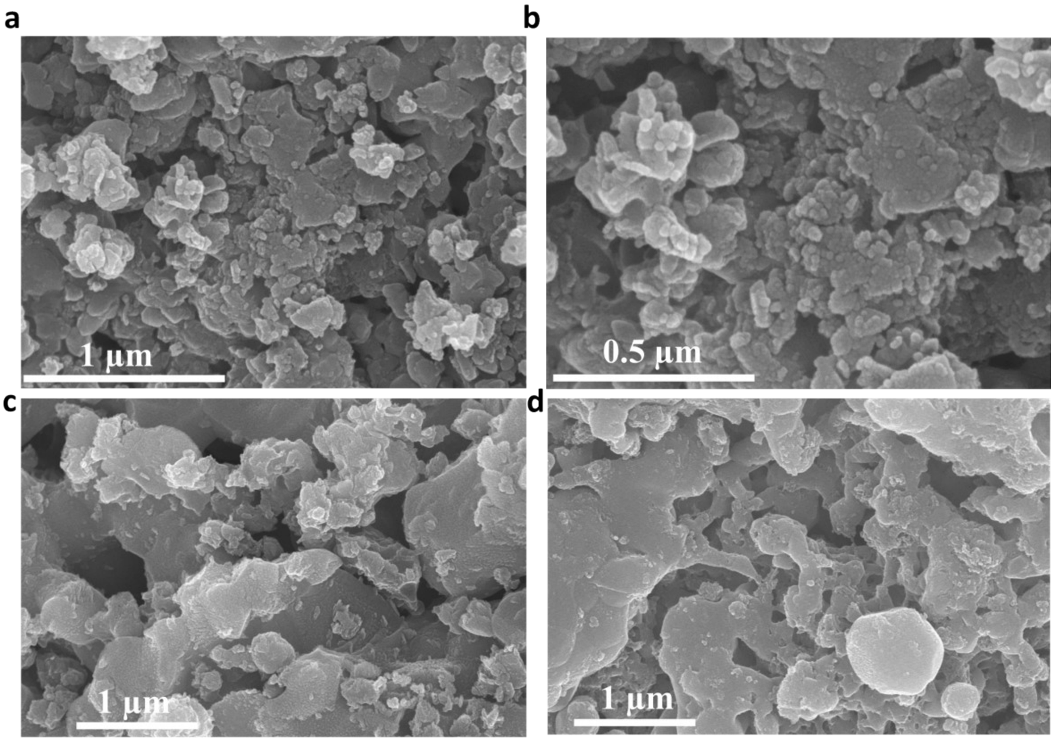

Fig. S5. FE-SEM image of NMVTP/C at (a) low and (b) high magnifications, FE-SEM image of (c) NMVFP/C and (d) NMVAP/C.

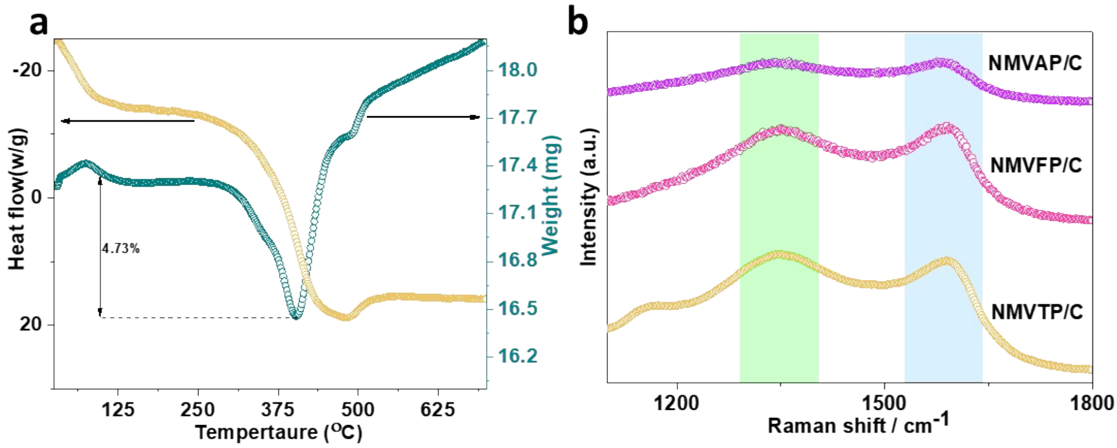

Fig. S6. (a) Thermogravimetric and (b) Raman spectra of the NMVTP/C, NMVFP/C, and NMVAP/C.

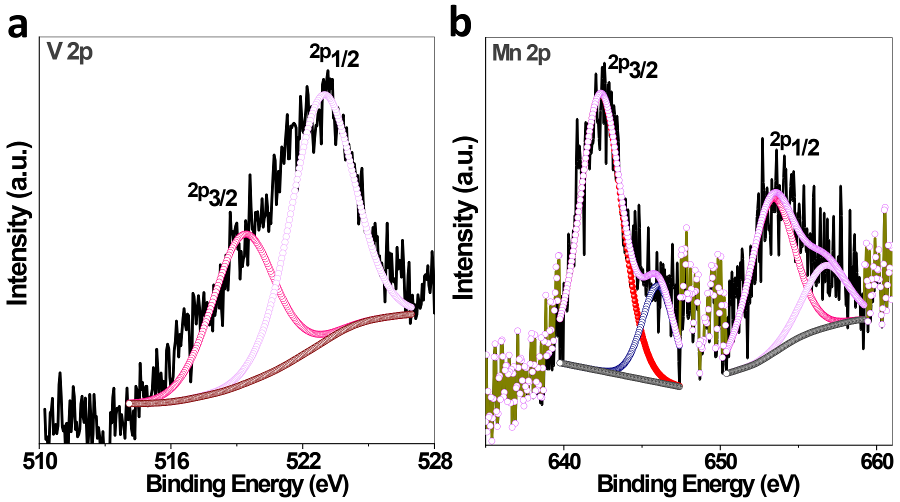

Fig. S7. XPS profile for NMVTP/C (a) V 2p and (b) Mn 2p.

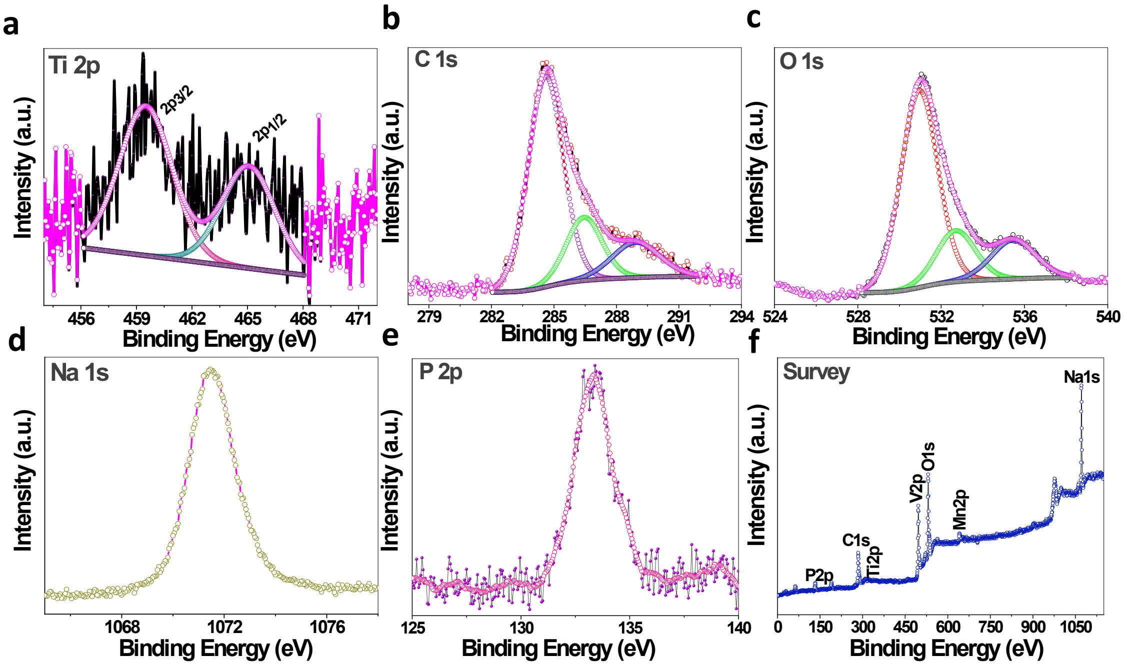

Fig. S8. XPS profile for NMVTP/C (a) Ti 2p, (b) C 1s, (c) O 1s, (d) Na 1s, (e) P 2p, and (f) survey spectrum.

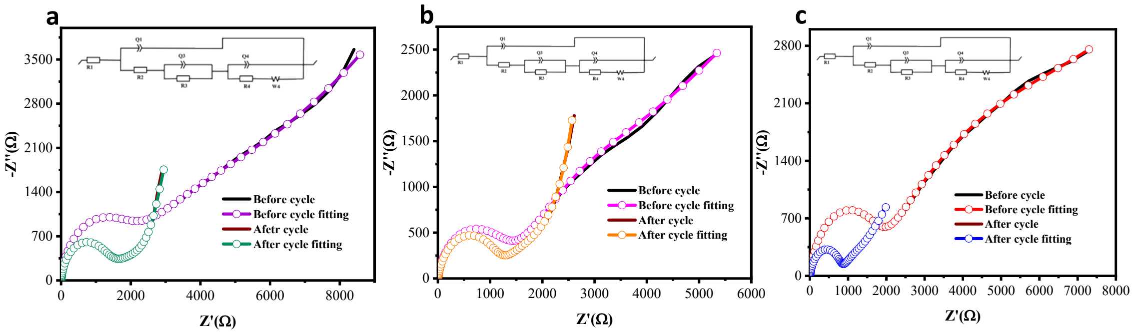

Fig. S9. Nyquist plot for a) NMVAP/C, b) NMVFP/C, and c) NMVTP/C (before and after cycling).

Table S3 The R1, R2, R3, R4, and W4 for NMVAP/C samples (before and after cycling).

Sample Name	R1 (Ω)	R2 (Ω)	R3 (Ω)	R4 (Ω)	W4 (Ω.S^-1/2)
Before cycle fitting	3.02	1925	11.6	1592	930.4
After cycle fitting	2.80	1386	0.5673	1025	365.1

Table S4 The R1, R2, R3, R4, and W4 for NMVFP/C samples (before and after cycling).

Sample Name	R1 (Ω)	R2 (Ω)	R3 (Ω)	R4 (Ω)	W4 (Ω.S^-1/2)
Before cycle fitting	3.32	487.2	7.536	1145	960.9
After cycle fitting	3.17	234.1	0.9478	485.8	414.1

Table S5 The R1, R2, R3, R4, and W4 for NMVTP/C samples (before and after cycling).

Sample Name	R1 (Ω)	R2 (Ω)	R3 (Ω)	R4 (Ω)	W4 (Ω.S^-1/2)
Before cycle fitting	3.60	1206	10.580	913.6	332.9
After cycle fitting	3.56	875.6	0.418	280.7	221.4

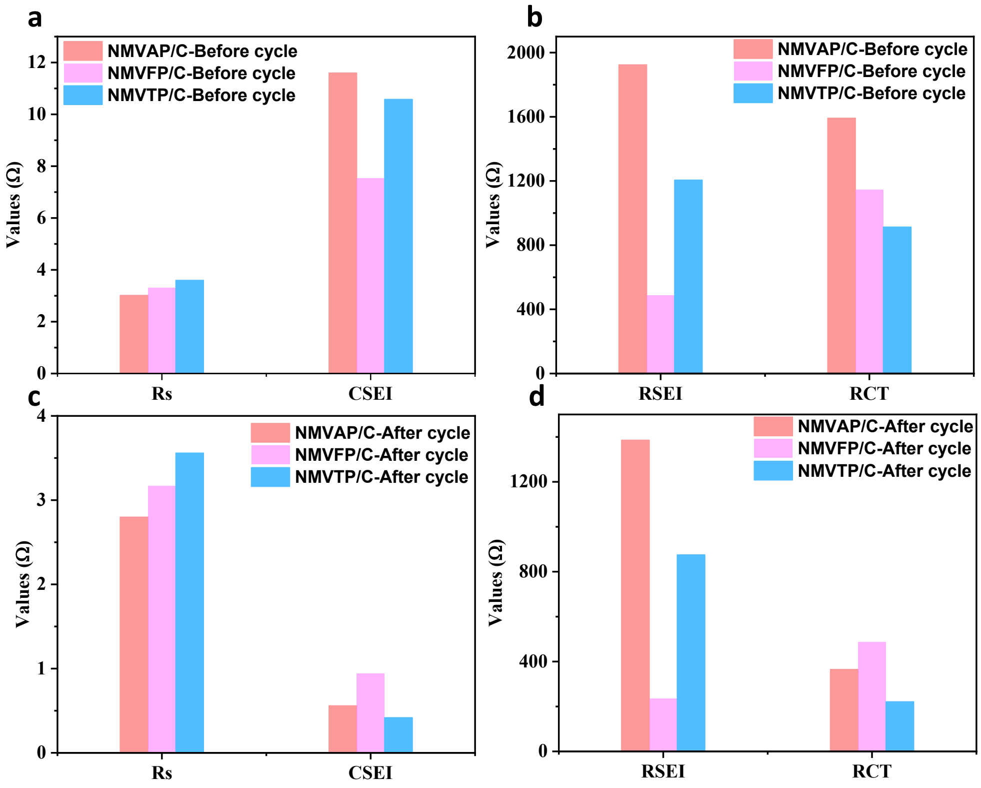

Fig. S10 Barchart comparing the resistance outputs of NMVAP/C, NMVFP/C, and NMVTP/C samples for a) Rs and C_{SEI}, values before the cycle, b) R_{SEI} and R_{CT} values before the cycle, c) Rs and C_{SEI}, values after the cycle,and d) R_{SEI} and R_{CT} values after the cycle.

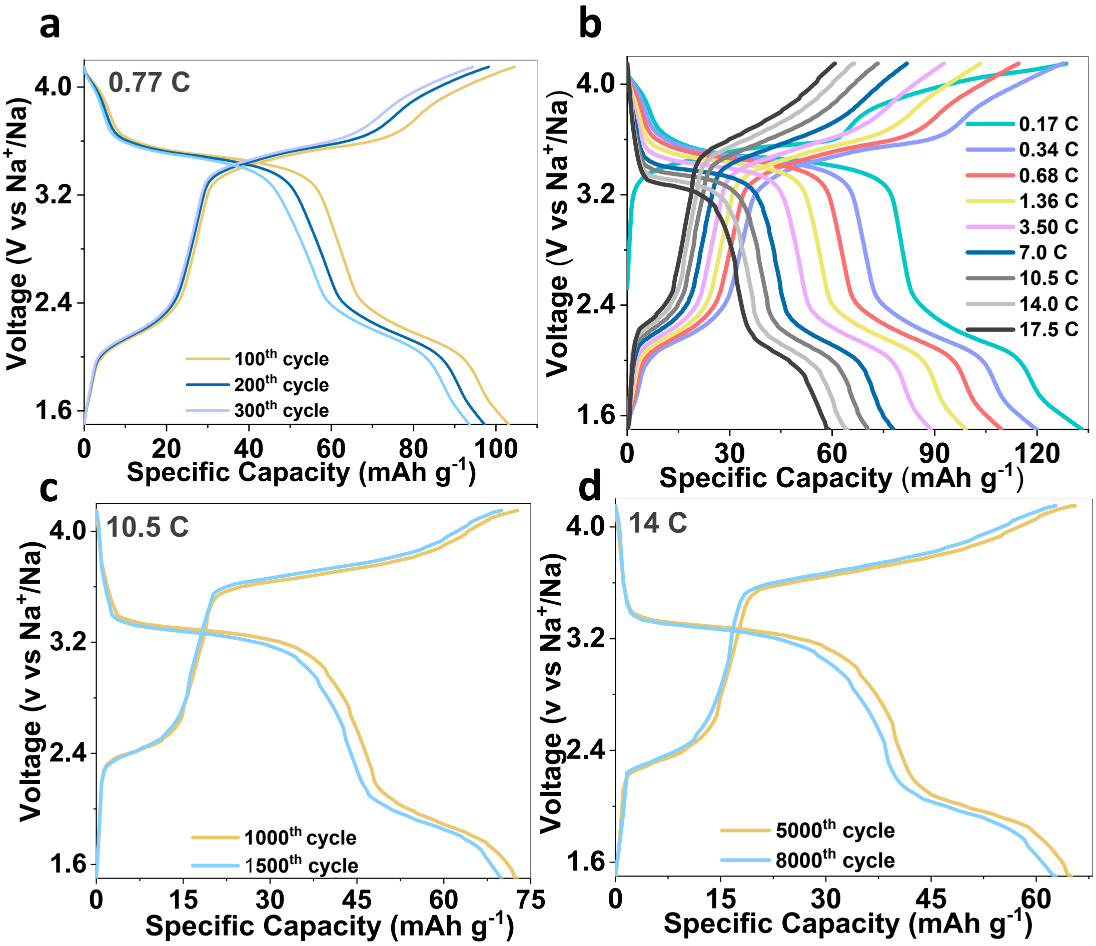

Fig. S11. Selected charge/discharge pattern for NMVTP/C at (a) 0.77 C. (b) Rate capability curve. (c) 10.5 C and (d) 14 C.

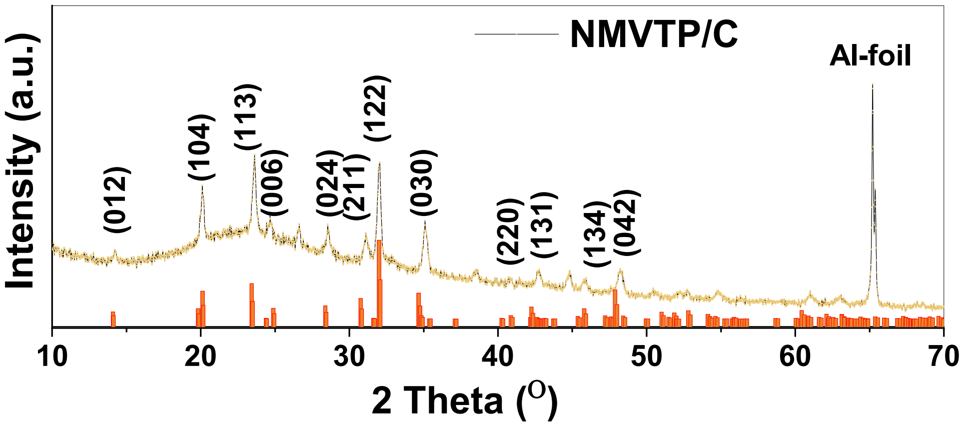

Fig. S12. *Ex situ* XRD patterns were obtained for the NMVTP/C cathode after the cycling process at 17C .

Table S6 Comparison of electrochemical performance between $Na_{3.5}MnV_{0.5}Ti_{0.5}(PO_4)_3$ with various NASICON-type cathodes that were recently reported.

Cathodes	Average Voltage (V vs. Na^+/Na)	Capacity	Cycling stability
$Na_4MnV(PO_4)_3$ [11]	3.45	101 mAh g^{-1} at 1 C (1 C= 110 mA g^{-1})	89 % at 1 C (1000 cycles)
$Na_4MnCr(PO_4)_3$ [12]	3.53	108 mAh g^{-1} at 0.1 C (1 C= 100 mA g^{-1})	58 % at 10 C (500 cycles)
$Na_3MnTi(PO_4)_3$ [13]	3.5	114 mAh g^{-1} at 20 C (1 C= 100 mA g^{-1})	81.2 % at 0.1 C (100 cycles)
$Na_3MnZr(PO_4)_3$ [14]	3.5	104 mAh g^{-1} at 0.1 C (1 C= 107 mA g^{-1})	91 % at 0.5 C (500 cycles)
$Na_3V_2(PO_4)_2F_3$ [15]	3.5	113 mAh g^{-1} at 0.5 C (1 C= 110 mA g^{-1})	98 % at 20 C (2000 cycles)
$Na_2VTi(PO_4)_3$ [16]	2.5	120 mAh g^{-1} at 0.5 C (1 C= 125 mA g^{-1})	86 % at 50 C (1000 cycles)
$Na_{3.5}MnV_{0.5}Al_{0.5}(PO_4)_3$ (Present work)	3.41	82 mAh g^{-1} at 0.17 C (1 C= 145.6 mA g^{-1})	N/A
$Na_{3.5}MnV_{0.5}Fe_{0.5}(PO_4)_3$ (Present work)	3.45	113.4 mAh g^{-1} at 0.17 C (1 C= 141.5 mA g^{-1})	N/A
$Na_{3.5}MnV_{0.5}Ti_{0.5}(PO_4)_3$ (Present work)	3.42	133.14 mAh g^{-1} at 0.17 C (1 C= 142.68 mA g^{-1})	75 % at 14 C (8000 cycles)

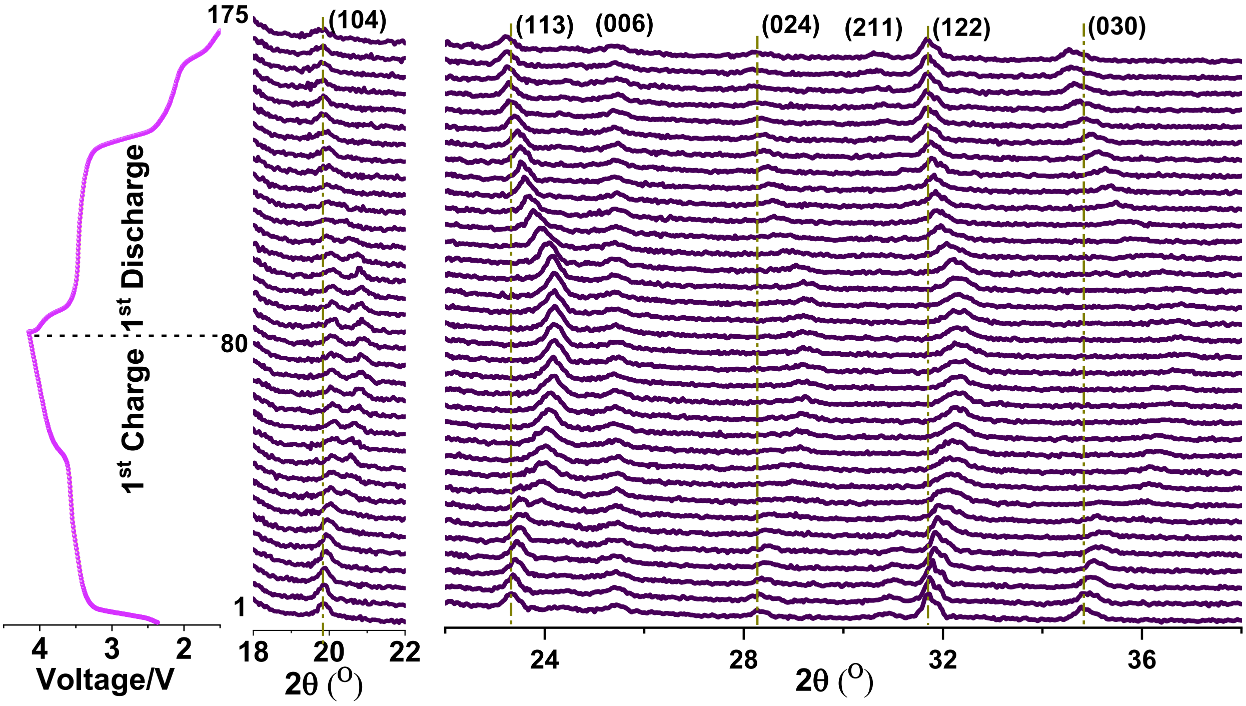

Fig. S13. *In situ* XRD pattern within the selected scanning region (a) 18-22° and (b) 23-40°, respectively.

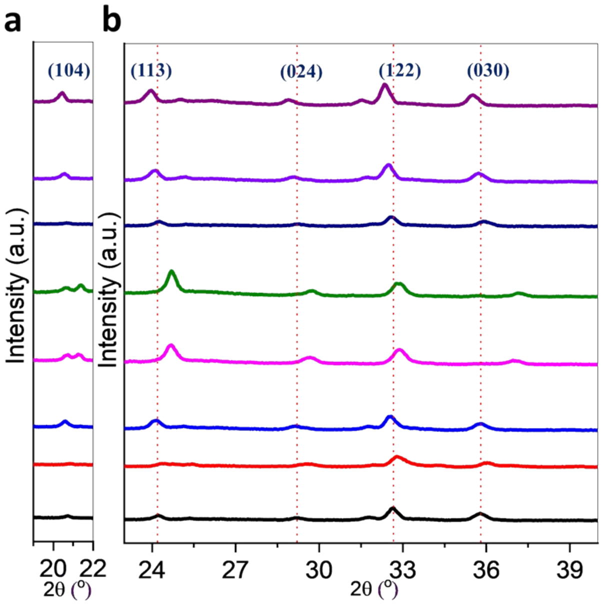

Fig. S14. *Ex situ* XRD patterns were obtained for the NMVTP/C cathode under different states of charge/discharge conditions (a) 19-22° and (b) 23-39.5°.

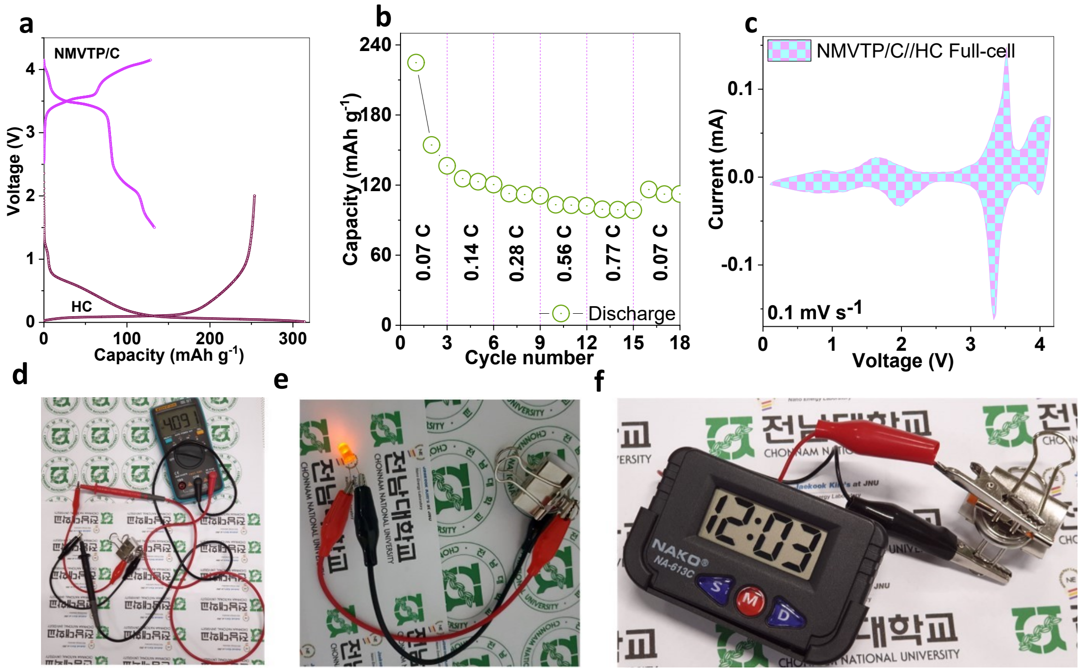

Fig. S15. Charge/discharge profile of the (a) NMVTP/C and HC half-cell. (b) Rate performance of NMVTP//HC full-cell. (c) CV profile of NMVTP//HC full-cell. (d) The cell voltage of NMVTP//HC full-cell. The NMVTP//HC full-cell powering (e) LED light and (f) digital watch.

References

1. P. Giannozzi, S. Baroni, N. Bonini, M. Calandra, R. Car, C. Cavazzoni, D. Ceresoli, G. L. Chiarotti, M. Cococcioni, I. Dabo, A. Dal Corso, S. De Gironcoli, S. Fabris, G. Fratesi, R. Gebauer, U. Gerstmann, C. Gougoussis, A. Kokalj, M. Lazzeri, L. Martin-Samos, N. Marzari, F. Mauri, R. Mazzarello, S. Paolini, A. Pasquarello, L. Paulatto, C. Sbraccia, S. Scandolo, G. Sclauzero, A. P. Seitsonen, A. Smogunov, P. Umari, R. M. Wentzcovitch, *J. Phys. Condens. Matter*, 2009, **21**, 395502.
2. J. P. Perdew, K. Burke, M. Ernzerhof, *Phys. Rev. Lett*. 1976, **77**, 3865.
3. H. J. Monkhorst, J. D. Pack, *Phys. Rev. B*. 1976, **13**, 5188.
4. C. G. BROYDEN, IMA *J. Appl. Math*. 1970, **6**, 76-90.
5. K. Okhotnikov, T. Charpentier, S. Cadars, *J. Cheminform*. 2016, **8**, 17.
6. L. Wang, T. Maxisch, and G. Ceder, Phys. Rev. B 73, 195107.
7. T. Tsuneda, and K. Hirao, WIREs Comput Mol Sci, 2014, **4**, 375-390.
8. K. Lin, Q. Liu, Y. Zhou, H. Chen, J. Liu, J. Zhao, X. Hou, Chem. Eng. J., 463 (2022), article 142464.
9. Holger-Dietrich Saßnick and Caterina Cocchi 2021 Electron. Struct. 3 027001.
10. L. L. Wong, K. C. Phuah, R. Dai, H. Chen, W. S. Chew, S. Adams, *Chem. Mater*. 2021, **33**, 625-641.

11. W. Zhou, L. Xue, X. Lü, H. Gao, Y. Li, S. Xin, G. Fu, Z. Cui, Y. Zhu and J. B. Goodenough, *Nano Lett*. 2016, **16**, 7836-7841.
12. W. Zhang, H. Li, Z. Zhang, M. Xu, Y. Lai, S.-L Chou, *Small*. 2020, **16**, 2001524.
13. H. Gao, Y. Li, K. Park, J. B. Goodenough, *Chem. Mater*. 2016, **28**, 6553-6559.
14. H. Gao, I. D. Seymour, S. Xin, L. Xue, G. Henkelman, J. B. Goodenough, *J. Am. Chem. Soc*. 2018, **140**, 18192.
15. Y. Jiang, X. Zhou, D. Li, X. Cheng, F. Liu, Y. Yu, *Adv. Energy Mater.* 2018, **8**, 1800068.
16. D. Wang, X. Bie, Q. Fu, D. Dixon, N. Bramnik, Y.-S. Hu, F. Fauth, Y. Wei, H. Ehrenberg, G. Chen, F. Du, *Nat. Commun*. 2017, **8**, 15888.